Ann Nucl Med (2015) 29:342–350
DOI 10.1007/s12149-015-0952-z

ORIGINAL ARTICLE

A performance comparison of novel cadmium–zinc–telluride camera and conventional SPECT/CT using anthropomorphic torso phantom and water bags to simulate soft tissue and breast attenuation

Chia-Ju Liu · Ju-Shin Cheng · Yi-Chieh Chen · Yih-Hwen Huang · Ruoh-Fang Yen

Received: 20 July 2014 / Accepted: 19 January 2015 / Published online: 28 January 2015

Abstract
Purposes This study was aimed to compare the physical performances of cadmium–zinc–telluride (CZT) camera and conventional Anger camera. An anthropomorphic torso phantom and water bags to simulate breasts were used to evaluate artifacts arising from soft tissue attenuation.
Materials and methods Linear source studies were performed to evaluate extrinsic resolution of CZT camera (Discovery NM 530c, GE) and conventional single-photon emission computed tomography (SPECT) Anger camera (Symbia T2, Siemens). Three sets of phantom experiments: cardiac phantom only (phantom H), anthropomorphic torso phantom added (phantom T), and torso phantom with water bags attached (phantom B), with Tc-99m were performed on both scanners. Imaging performances were evaluated through count sensitivity, contrast-to-noise ratio, quantitative sharpness profile, wall thickness, perfusion uniformity (measured by standard deviation of perfusion percentage of 20 segments using quantitative perfusion SPECT (QPS) software, Cedars-Sinai), and visual imaging quality (using 20-segment sum defect scores (SDS) of QPS) for CZT camera, conventional SPECT without and with computed tomography transmission attenuation correction (AC).
Results CZT cameras had higher extrinsic resolution than conventional SPECT. Myocardium count sensitivity of CZT camera is about threefold of conventional SPECT. Contrast-to-noise ratios and sharpness profiles are higher on CZT camera but degraded while extracardiac soft tissue presented. Myocardial walls measured on CZT images were thicker. Images of CZT had lower SDS, while AC reduced the differences of SDS between CZT and CC. Perfusion images from CZT had the better uniformity than SPECT without or with AC. Breast attenuation was less prominent on CZT camera than conventional SPECT, while inferior and inferolateral segments still suffer marked soft tissue attenuation on CZT camera.
Conclusions CZT camera has better physical performance and image quality with less artificial perfusion defects than conventional SPECT. CZT camera also has less breast attenuation than conventional SPECT. However, extracardiac soft tissue may degrade the superior performance of CZT camera, and attenuation correction methods are still needed to solve the attenuation issues in inferior and inferolateral myocardium.

Keywords Myocardial perfusion imaging · CZT camera · Conventional SPECT · Soft tissue attenuation

Electronic supplementary material The online version of this article (doi:10.1007/s12149-015-0952-z) contains supplementary material, which is available to authorized users.

C.-J. Liu · J.-S. Cheng · Y.-C. Chen · Y.-H. Huang · R.-F. Yen (✉)
Department of Nuclear Medicine, National Taiwan University Hospital, No. 7, Chung-Shan South Road, Taipei 100, Taiwan
e-mail: rfyen@ntu.edu.tw

R.-F. Yen
Molecular Imaging Center, National Taiwan University, Taipei, Taiwan

Introduction

The myocardial perfusion imaging (MPI) is the most widely used non-invasive cardiac imaging tool for diagnosis and prognosis of coronary artery disease. However, the conventional myocardial single-photon emission computed tomography (SPECT) using Anger cameras has been criticized for its poor energy resolution, long acquisition time, high radiation doses, and low spatial resolution. The

cadmium–zinc–telluride (CZT) semiconductors were introduced into SPECT myocardial perfusion imaging in recent few years. The novel gamma camera not only equips with CZT technique but also has specialized array of pinhole gamma cameras with heart-oriented geometry. The higher energy resolution of CZT allows shorter acquisition time and provides higher spatial resolution. Several studies compared the performance of CZT with conventional Anger camera. The advancement of CZT SPECT was proven to have highly correlated diagnostic performance [1–8] with reduced dose of isotope [9–14], shorter acquisition time [15], and better imaging quality comparing with conventional gamma camera. Clinical validation with results of invasive coronary angiography (CAG) has also been confirmed [16, 17]. Its characteristics of heart-oriented geometry and higher energy resolution are expected to reduce the soft tissue attenuation. However, the performance of novel CZT under effects of soft tissue attenuation still needs validation. Only limited studies used standardized phantoms to simulate the possible effects of soft tissue on CZT [2, 18, 19], and all of them focused on the subdiaphragmatic soft tissue attenuation using torso phantoms. Phantom study to simulate the attenuation effects from breasts has not been well studied yet. The aim of this study is using phantoms to compare the performance of novel CZT with conventional Anger type dual-head camera system (Anger camera) under influences of both subdiaphragmatic soft tissue and breasts.

Materials and methods

SPECT imaging

CZT SPECT (CZT)

The CZT, the Discovery NM530c (GE Healthcare, Haifa, Israel), is equipped with fixed nineteen CZT detectors and collimation over an arc of 180° and oriented to the heart region. Projections are recorded on the 32 × 32 pixelated (2.46 × 2.46 mm) CZT elements. Maximum likelihood expectation maximization was used with reconstructed voxel size 4.0 × 4.0 × 4.0 mm. A Butterworth post-processing filter was applied (order 10, cut-off frequency 0.37) to the reconstructed slices. Acquisition time for each phantom was 10 min.

Conventional Anger camera SPECT (Anger camera)

The conventional Anger camera system used is Symbia T2 (Siemens Medical Solution Inc., IL, USA), which is a dual-head single-photon emission computed tomography (SPECT)/computed tomographic (CT) scanner. Imaging acquisition is using high energy collimators with noncircular 180° acquisition for 64 projections at 30 s per projection. Data are stored in a 128 × 128 matrix. Images are reconstructed with ordered set expectation maximization iterative algorithms (4 iteration, 8 subsets). The reconstructed voxel size is 4.8 × 4.8 × 4.8 mm. A Gaussian processing filter was applied (full width at half maximum = 8.4 mm) to the reconstructed slices. A low-dose CT was also acquired for attenuation correction (130 kV, 17 mAs, pitch 1.5 mm, slice thickness 5 mm). Images reconstructed with or without attenuation were both performed. Acquisition time of SPECT for each phantom was 20 min.

Linear source study for extrinsic spatial resolution

To compare the extrinsic spatial resolution of two different camera systems, images of linear sources with 1.1 mm internal diameter filled with 2 MBq/mL ^{99m}Tc were acquired. Three linear sources were placed at the parallel edges of a cube; each was 75 mm in distance. Images of linear sources were acquired in cephalocaudal direction and placed in the anterior, central and right lateral positions of the imaging fields of two camera systems. Horizontal profiles of middle slice of each linear source were analyzed with AMIDE software. The spatial resolution was determined as the full width at half maximum (FWHM) of Gaussian fit.

Phantom studies

Cardiac phantom (phantom H)

A commercial cardiac phantom (ECT/CAR/I, Data Spectrum Corporation, NC, USA) was used to mimic the left ventricle of a normal heart. The mimicked ventricle wall was 24 mm in thickness and filled with water containing 9.7 MBq ^{99m}Tc. The cardiac phantom was positioned with 25° deviation of the apex from the craniocaudal orientation to simulate the normal orientation in human.

Torso phantom (phantom T)

An anthropomorphic torso phantom (Data Spectrum Corporation, NC, USA) was used to model male patients. Heart, background, lungs, and liver compartments were filled with 9.7, 106.6, 1.3, and 43.3 MBq ^{99m}Tc, respectively.

Breast phantom (phantom B)

Two water bags, each filled with 500 ml normal saline and 2.8 MBq ^{99m}Tc, were attached to the anterior side of torso phantom. The phantom was used to simulate breasts in female patients.

Data analysis

The following parameters were calculated to evaluate the performance of both CZT and Anger camera.

Count sensitivity

Total count sensitivity was compared between two cameras and calculated as total recording counts divided by recording time and then by filled activity within the phantoms. For each phantom in CZT and Anger camera, a frame with anterior view was chosen and a region of interest (ROI) was drawn on cardiac insert. Ratio of counts of that ROI divided by total counts of that frame was calculated. Total acquired counts were then multiplied by the ratio of counts of ROI/total field counts and gave estimated cardiac activity [4].

Contrast-to-noise ratio

Mid-ventricle short-axis slices were selected from each set of images to determine contrast-to-noise ratio. A ring-shaped region of interest confining entire lateral myocardial wall was used for myocardium counts. A square region of interest (15 mm × 15 mm) was placed within ventricle and the count within the region was considered noise.

Sharpness profile

A horizontal profile was also selected on the same mid-ventricular short-axis slice. After filtering the lower quarter of myocardium counts, the maximal slope of myocardium count on the epicardial border of lateral wall was calculated as quantitative sharpness on the selected profile.

Wall thickness

Wall thickness was estimated by the pixel number of horizontal or vertical profiles of each wall multiplied by corresponding pixel sizes of two camera systems.

Uniformity

The SPECT images were analyzed with quantitative-gated SPECT (QGS) (Cedars Sinai Medical Center, Los Angeles, CA, USA). The myocardium was divided into 20 segments. Tracer uptake of each myocardial segment was quantified using normalized percentage of maximum myocardial uptake. The standard deviations of 20 segments were calculated to compare the uniformity of reconstructed images of two different camera systems.

Visual assessment

The perfusion defects were also visually evaluated on 10-color scale using 5-point scoring system (0 = normal, <20 % perfusion defects; 1 = mildly abnormal, >20 % perfusion defects; 2 = moderately abnormal, >40 % perfusion defects; 3 = severely abnormal, >60 % perfusion defects; and 4 = absent perfusion, >80 % perfusion defects or no uptake) by one experienced nuclear medicine physician. The summed score was obtained to compare the extent of perfusion defects. The tracer distribution patterns of two camera systems using polar maps generated by QGS were also visually compared.

Results

Spatial resolution

The FWHM of linear sources for each camera is listed in Table 1. The linear source analysis showed overall better spatial resolution of the CZT than that of the Anger camera. With CZT, the linear source put in anterior position had best spatial resolution, followed by the central linear source. The right lateral linear source, which was put in the furthest distant from the arc of CZT, had the worst spatial resolution. With Anger camera, the linear source in right lateral position had best spatial resolution than those in anterior and central positions.

Count sensitivity

The total count sensitivity of three phantoms and the estimated myocardial count sensitivity are shown in Fig. 1. The CZT showed consistently higher total count and estimated myocardium sensitivity than the Anger camera. The total count sensitivity of the CZT in phantom H was 3.2-fold of that of the Anger camera. While extracardiac activity was present, such as in phantom T and phantom B, the CZT demonstrated higher total count sensitivity than Anger camera in lesser degree (1.6 and 1.5 fold, respectively). While myocardium count sensitivity of the phantom T and phantom B were estimated using regions of

Table 1 The spatial resolution with linear sources

Full width at half maximum (mm)	Anterior position	Central position	Right lateral position
CZT camera	5.47	6.34	6.81
Anger camera	12.17	12.46	10.66

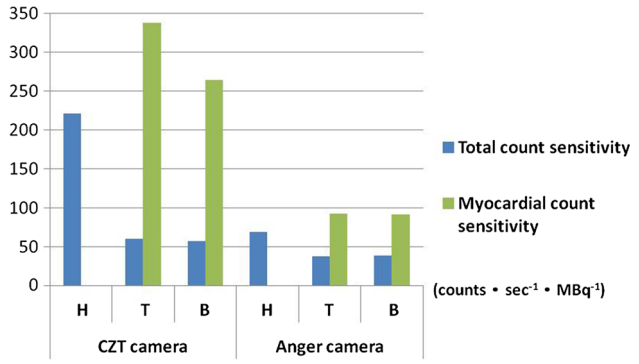

Fig. 1 The comparison of the total count sensitivity and myocardium count sensitivity between CZT and Anger cameras. Results demonstrated higher count sensitivity of CZT. Even under the effect of extracardiac soft tissue, the estimated myocardium count sensitivity was consistently about threefold with the CZT camera

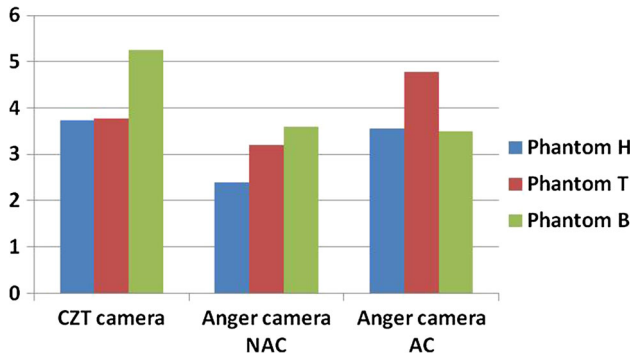

Fig. 2 The comparison of the contrast-to-noise ratios between CZT and Anger cameras. Generally, CZT camera had higher ratios than Anger camera. When thoracic soft tissue attenuation was prominent (in case of phantom T), however, CT attenuation improved the contrast-to-noise ratio of Anger camera, which was even superior than that of CZT

interest, CZT showed similarly about threefold of myocardium count sensitivity than the Anger camera (phantom T: 3.6-fold, phantom B: 2.8-fold).

Contrast-to-noise ratio

The contrast-to-noise ratios of two cameras are shown in Fig. 2. CZT showed best contrast-to-noise ratio with phantom H and phantom B. However, with phantom T, Anger camera with attenuation correction showed the best contrast-to-noise ratio, followed by CZT.

Sharpness profile

Sharpness profile analysis is shown in Fig. 3. CZT had sharpest profile with phantom H and phantom T, but slightly less sharp than Anger camera without attenuation in phantom B.

Wall thickness

The reconstructed myocardium wall thickness is shown in Fig. 4. Wall thickness estimated through reconstructed images of CZT tends to have thicker myocardium walls, except in the case of phantom B. The inferior wall thickness of phantom B obtained from Anger camera with attenuation correction was thicker than that from CZT.

Uniformity

The standard deviations of overall myocardial tracer uptake with different cameras are listed in Table 2. The CZT consistently showed superior uniformity over the Anger camera with and without attenuation correction.

Visual assessment

The polar maps of each camera systems are demonstrated in Fig. 5.

With phantom H, the tracer activity patterns were similar in two camera systems. The anterior and apical inferior myocardium had relative higher tracer distribution, while apex, septum, and lateral myocardium had decreased tracer distribution. However, the Anger camera with AC had higher inferior myocardium uptake in phantom T and phantom B.

The normalized tracer uptake percentages of separate myocardial segments using different cameras are shown in Fig. 6. With phantom T, the CZT still suffered soft tissue attenuation within all segments. Most myocardial segments on the Anger camera without AC were attenuated more than those on the CZT except inferior and inferolateral segments. The normalized uptake percentage at inferior and inferolateral segments on the CZT was lower than that on the Anger camera. Attenuation correction largely restored the activity loss in inferior and inferolateral segments and had highest normalized uptake percentage. However, the normalized uptake percentage of apex on the Anger camera fell significantly after attenuation correction.

When radioactive water bags were added, as in phantom B, the anterior and anteroseptal segments still had preserved high normalized uptake percentage on the CZT unlike the significant activity loss in these areas on Anger camera. Furthermore, the attenuation at inferior and inferolateral segments on the CZT became less prominent with phantom B, although the attenuation correction could regain the uptake percentage of inferior and inferolateral segments on Anger camera. The overall uptake pattern was more homogenous on the CZT.

The summed scores of perfusion defects by visual interpretation are listed in Table 3. The summed scores of visual perfusion defects were less in CZT than Anger

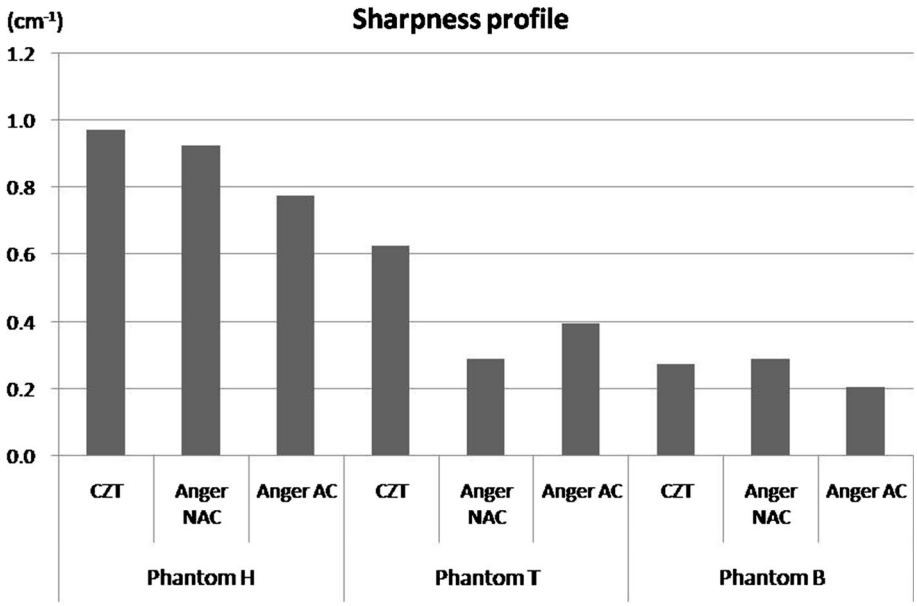

Fig. 3 The comparison of the sharpness profile analysis between CZT and Anger cameras. CZT camera had sharpest profile on phantom H and phantom T, but the sharpness was affected by simulated breast (phantom B) and lower than that of the Anger camera

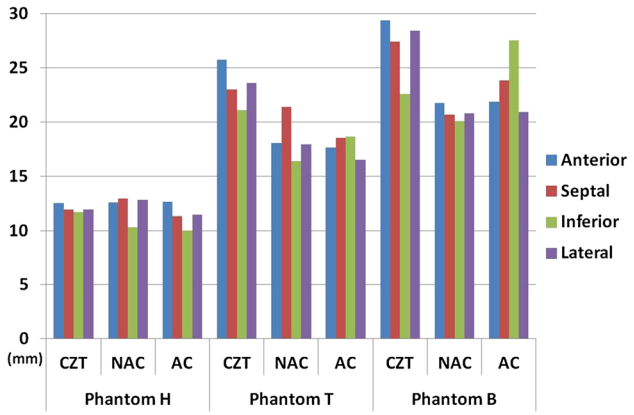

Fig. 4 The reconstructed myocardium wall thickness on two kinds of cameras. Wall thickness estimated through reconstructed images of CZT camera tends to have thicker myocardium walls, except in the case of phantom B

Table 2 The standard deviation of overall myocardial tracer uptake

Standard deviation	CZT	Anger camera (NAC)	Anger camera (AC)
Phantom H	6.2	7.8	7.1
Phantom T	12.4	15.6	14.2
Phantom B	9.3	9.4	9.7

camera with and without attenuation correction. Imaging of phantom B using the Anger camera with attenuation correction diminished the perfusion defects and had equal summed scores as using the CZT.

Discussion

In this study, the CZT demonstrated the superior spatial resolution using linear source analysis. The linear source in anterior position, which is closest to the majority of pinhole cameras, had best spatial resolution. In contrast, the worst spatial resolution of the linear source put in the right lateral position may be explained by its furthest distant from the camera arc. Therefore, it is worthy of notice to position patients as close as the camera arc in clinical practice.

The CZT has higher count sensitivity than Anger camera (Fig. 1). The overall increased count sensitivity was less prominent with simulated extracardiac background activity, which is compatible with the concentralized imaging field toward cardiac region designed in the CZT. Nevertheless, the estimated myocardium count sensitivity was consistently about threefold with the CZT.

The better performance of the CZT was also manifested by higher contrast-to-noise ratio on reconstructed images. However, it was notable that the contrast-to-noise ratio of phantom T using CZT was less than that obtained from Anger camera after attenuation correction. This may be explained by the marked attenuation artifact at inferolateral wall, which was noted on CZT but corrected by AC on conventional camera.

The sharpness profile analysis demonstrated that reconstructed myocardium from the CZT was characterized by sharper border, partially due to the better spatial resolution of the CZT. However, this phenomenon was not observed as background activity increased, especially with simulated breasts. The sharper myocardium wall is not only

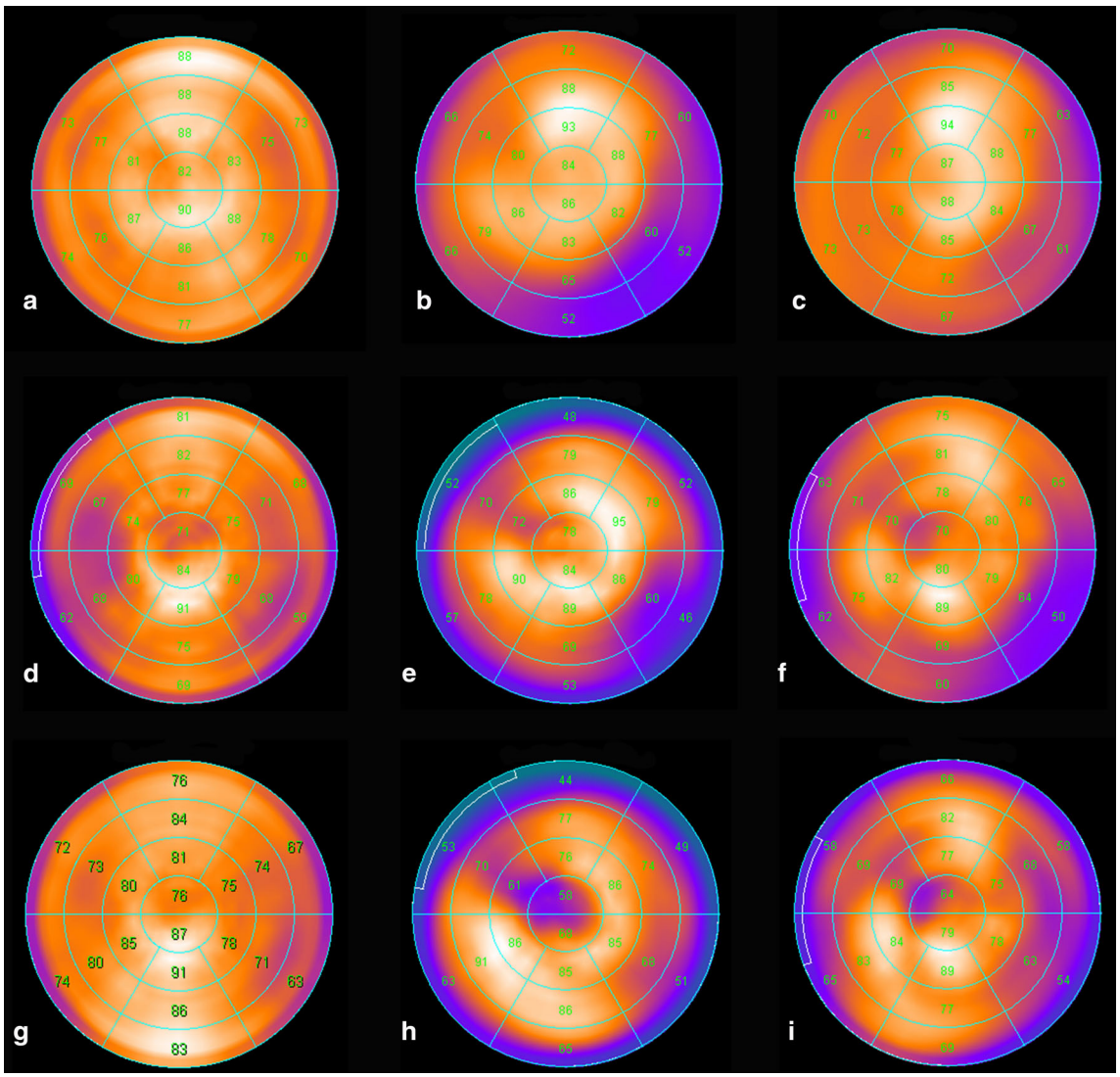

Fig. 5 The 20-segment polar maps of each camera systems were displayed. Numbers within each segment stand for average uptake percentage of corresponding segments. *Top row* (**a–c**) from *left* to *right*: phantom H, T and B on CZT camera, respectively. *Middle row* (**d–f**) from *left* to *right*: phantom H, T and B on Anger camera without attenuation correction. *Lower row* (**g–i**) from *left* to *right*: phantom H, T and B on Anger camera with CT attenuation correction. With phantom H, the tracer activity patterns were similar to pattern of self attenuation in two camera systems. With extracardiac soft tissue, inferior myocardial activity loss was compensated by CT attenuation correction on Anger camera. Lateral wall myocardium suffered prominent activity loss on both camera systems, especially on Anger camera without CT correction

attributed to the differences of spatial resolution but also detector designs and reconstruction methods of two camera systems. It could be assumed that the sharpness of myocardium images obtained with the CZT is degraded when background soft tissue activity is prominent such as in obese or female patients.

The reconstructed myocardium wall thickness of phantom H was similar on both cameras. However, the reconstructed images with the CZT tended to have thicker myocardium walls as background extracardiac activity increased. Besides, it was observed that attenuation correction could increase the thickness of inferior wall. We attributed the difference of wall thickness to the scattered extracardiac activity. The different filters chosen on two camera systems largely affected the wall thickness.

Surprisingly, marked perfusion defects were observed when normal cardiac phantom H was used in both camera systems (Fig. 5a, d). The septal and lateral myocardial walls tend to have lower recorded counts. Lower activity toward basal portion of each segment from apex was also observed. The inhomogeneous recorded tracer activity may be explained by the position of imaged objects within field of view and their relative distance from detectors of camera. Furthermore, the pattern of recorded activity on

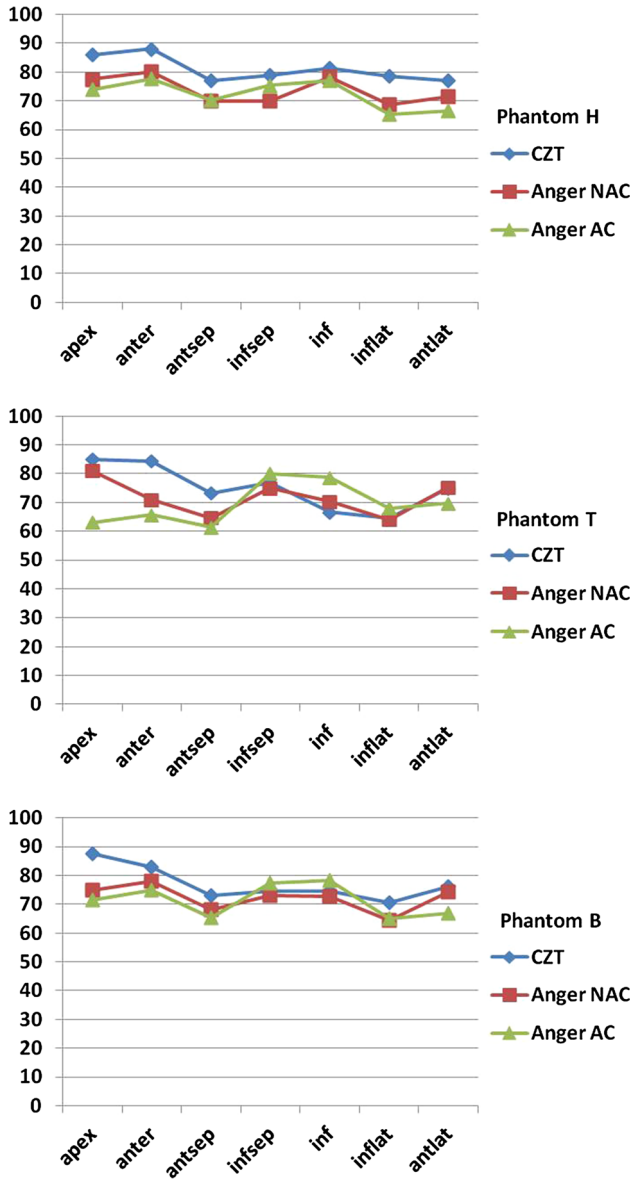

Fig. 6 Normalized uptake percentages of myocardium segments. *Anter* anterior wall, *antsep* anteroseptal wall, *infsep* inferoseptal wall, *inf* inferior wall, *inflat* inferolateral wall, *antlat* anterolateral wall. The figure demonstrated the change of segmental uptake percentage under the effects of extracardiac soft tissue. The CZT camera still suffered activity loss at all segments due to extracardiac soft tissue, worst at inferior and inferolateral segments. Most myocardial segments on the Anger camera without AC were attenuated more than those on the CZT camera except inferior and inferolateral segments (Anger NAC T–H, Anger NAC B–H). Attenuation correction largely restored the activity loss in inferior and inferolateral segments on Anger camera and had highest normalized uptake percentage (inf and inflat of Anger AC T–H, Anger AC B–H). *T–H* the difference of uptake percentage between phantom T and phantom H, *B–H* the difference of uptake percentage between phantom B and phantom H

phantom H differed in both cameras. Anterior wall had highest activity on CZT, while apical inferior segment had highest activity on Anger camera. This is probably due to

Table 3 The summed scores of perfusion defects by visual interpretation

Summed defect score (% myocardium)	CZT	Anger camera (NAC)	Anger camera (AC)
Phantom H	8 (10 %)	13 (16.3 %)	12 (15 %)
Phantom T	9 (11.3 %)	10 (12.5 %)	10 (12.5 %)
Phantom B	12 (15 %)	14 (17.5 %)	12 (15 %)

different gantry design, and angles of cameras in both systems superimposed the difference in segmental recorded counts. In combination with our results of linear source resolution, we assume that there should be a best acquisition position of CZT with highest recorded activity and resolution, which is probably at the center of bed and close to the camera arm. The importance of patient positioning when using CZT is confirmed in a recent study [20].

The tracer distribution patterns of cardiac phantom were similar on two camera systems. When extracardiac soft tissue presented, however, the tracer uptake pattern differed characteristically on two camera systems. The reconstructed images with CZT were more homogenously visually, but the significant activity loss of inferior and inferolateral walls on phantom T was not avoided with the use of CZT. This could be explained by two reasons. First, the low row of pinhole collimators of NM530c looking up to at the heart detects the inferior and inferolateral walls through the subdiaphragmatic soft tissue and causes activity loss. Second, the inferior and inferolateral segments are actually the furthest myocardium from the camera arc of NM530. Both may result in the lower counts of the inferior and inferolateral segments. When extracardiac soft tissue presented, the count loss at these segments became more prominent. The angular longitudinal acquisition of pinhole cameras at low row may record less counts through extracardiac soft tissue, while Anger camera recorded counts through lung and had less attenuation with focally increased activity at these areas. The attenuation correction technique with low-dose CT can largely restore the lost activity. However, the restored activity of inferoseptal and inferior walls with attenuation correction may be overly compensated and become the highest uptake portion of myocardium. This over correction may lead to the resultant focal defect at apex after myocardium uptake normalization.

With water bags attached to simulate breasts, the overall tracer distribution became more homogenous on CZT. This was probably because the imaged phantom became cylinder instead of elliptic in shape. The heart-oriented geometry of the CZT arc recorded radioactivity through more equally distributed soft tissue. The diminished difference of attenuation between anterior and inferolateral segments made uptake pattern more homogenous.

Despite presented perfusion defects, the reconstructed images of the CZT still had better overall visual uniformity than the Anger camera no matter simulated extracardiac soft tissue existed or not. This better uniformity of the CZT was substantiated by calculated standard deviation of tracer uptake percentage in this study. Our study also demonstrated that CZT had fewer artifacts than Anger camera with less SDS.

In summary, our study confirmed that CZT camera has better photon sensitivity, higher spatial resolution, and superior image quality than the conventional Anger camera as previous phantom studies have shown [2, 18]. However, it is found that there still are noticeable effects of extracardiac soft tissue attenuation on CZT, which degrade the image quality of CZT such as sharpness and contrast-to-noise ratio. It has been observed that CZT may not perform as well in obese patients [1, 21]. Our phantom study may substantiate the role of soft tissue activity in these clinical observations. Most importantly, the inferior and inferolateral myocardium still suffers significant soft tissue attenuation in our study. These myocardial segments are supplied by either right coronary artery (RCA) or left circumflex artery (LCX). The performance and diagnostic accuracy of CZT regarding RCA and LCX remained unclear. The mild discordance in RCA territory was found between CZT and Anger camera with more severe defects on CZT [3]. Gimelli et al. [8] observed that CZT had higher accuracy in RCA and LCX territories but obese patients lowered the accuracy in LCX territory [22]. In addition, Fiechter et al. [21] found that Anger camera had better image quality on obese patients with higher body mass index. The attenuation correction of CZT may use either CT [13, 23–25] or breath hold method [26]. Our results substantiated the need of attenuation correction. In contrast, compared with Anger camera, artificial artifacts from breasts may be less prominent with novel CZT. Breast attenuation contributes largely to the reduced accuracy of MPI in women. A recent study confirmed the well performance of CZT camera in female patients [27].

Conclusion

The novel CZT has better imaging performance than the Anger camera. Fewer artifacts are noted on CZT when breast attenuation presents. However, extracardiac soft tissue activity can still hamper the image quality such as sharpness and contrast-to-noise ratio. False positive results may arise in inferior and inferolateral segments. The results of this phantom study should be further corroborated in clinical observation on patients and correlate with coronary angiographic findings. If so, attenuation correction to solve this problem will be warranted.

Acknowledgments The study was supported in part by grant NTUH.104-N01 from the National Taiwan University Hospital, Taipei, Taiwan.

References

1. Verger A, Djaballah W, Fourquet N, Rouzet F, Koehl G, Imbert L, et al. Comparison between stress myocardial perfusion SPECT recorded with cadmium–zinc–telluride and Anger cameras in various study protocols. Eur J Nucl Med Mol Imaging. 2013;40:331–40.
2. Imbert L, Poussier S, Franken PR, Songy B, Verger A, Morel O, et al. Compared performance of high-sensitivity cameras dedicated to myocardial perfusion SPECT: a comprehensive analysis of phantom and human images. J Nucl Med. 2012;53:1897–903.
3. Tanaka H, Chikamori T, Hida S, Uchida K, Igarashi Y, Yokoyama T, et al. Comparison of myocardial perfusion imaging between the new high-speed gamma camera and the standard anger camera. Circ J. 2013;77:1009–17.
4. Songy B, Lussato D, Guernou M, Queneau M, Geronazzo R. Comparison of myocardial perfusion imaging using thallium-201 between a new cadmium–zinc–telluride cardiac camera and a conventional SPECT camera. Clin Nucl Med. 2011;36:776–80.
5. Buechel RR, Herzog BA, Husmann L, Burger IA, Pazhenkottil AP, Treyer V, et al. Ultrafast nuclear myocardial perfusion imaging on a new gamma camera with semiconductor detector technique: first clinical validation. Eur J Nucl Med Mol Imaging. 2010;37:773–8.
6. Esteves FP, Raggi P, Folks RD, Keidar Z, Askew JW, Rispler S, et al. Novel solid-state-detector dedicated cardiac camera for fast myocardial perfusion imaging: multicenter comparison with standard dual detector cameras. J Nucl Cardiol. 2009;16:927–34.
7. Sharir T, Ben-Haim S, Merzon K, Prochorov V, Dickman D, Berman DS. High-speed myocardial perfusion imaging initial clinical comparison with conventional dual detector anger camera imaging. JACC Cardiovasc Imaging. 2008;1:156–63.
8. Gimelli A, Bottai M, Giorgetti A, Genovesi D, Kusch A, Ripoli A, et al. Comparison between ultrafast and standard single-photon emission CT in patients with coronary artery disease: a pilot study. Circ Cardiovasc Imaging. 2011;4:51–8.
9. Nakazato R, Berman DS, Hayes SW, Fish M, Padgett R, Xu Y, et al. Myocardial perfusion imaging with a solid-state camera: simulation of a very low dose imaging protocol. J Nucl Med. 2013;54:373–9.
10. Oddstig J, Hedeer F, Jogi J, Carlsson M, Hindorf C, Engblom H. Reduced administered activity, reduced acquisition time, and preserved image quality for the new CZT camera. J Nucl Cardiol. 2013;20:38–44.
11. Songy B, Guernou M, Lussato D, Queneau M, Geronazzo R. Low-dose thallium-201 protocol with a cadmium–zinc–telluride cardiac camera. Nucl Med Commun. 2012;33:464–9.
12. Gimelli A, Bottai M, Genovesi D, Giorgetti A, Di Martino F, Marzullo P. High diagnostic accuracy of low-dose gated-SPECT with solid-state ultrafast detectors: preliminary clinical results. Eur J Nucl Med Mol Imaging. 2012;39:83–90.
13. Nkoulou R, Pazhenkottil AP, Kuest SM, Ghadri JR, Wolfrum M, Husmann L, et al. Semiconductor detectors allow low-dose-low-dose 1-day SPECT myocardial perfusion imaging. J Nucl Med. 2011;52:1204–9.
14. Duvall WL, Croft LB, Godiwala T, Ginsberg E, George T, Henzlova MJ. Reduced isotope dose with rapid SPECT MPI imaging: initial experience with a CZT SPECT camera. J Nucl Cardiol. 2010;17:1009–14.

15. Duvall WL, Croft LB, Ginsberg ES, Einstein AJ, Guma KA, George T, et al. Reduced isotope dose and imaging time with a high-efficiency CZT SPECT camera. J Nucl Cardiol. 2011;18:847–57.
16. Duvall WL, Sweeny JM, Croft LB, Ginsberg E, Guma KA, Henzlova MJ. Reduced stress dose with rapid acquisition CZT SPECT MPI in a non-obese clinical population: comparison to coronary angiography. J Nucl Cardiol. 2012;19:19–27.
17. Duvall WL, Sweeny JM, Croft LB, Barghash MH, Kulkarni NK, Guma KA, et al. Comparison of high efficiency CZT SPECT MPI to coronary angiography. J Nucl Cardiol. 2011;18:595–604.
18. Takahashi Y, Miyagawa M, Nishiyama Y, Ishimura H, Mochizuki T. Performance of a semiconductor SPECT system: comparison with a conventional Anger-type SPECT instrument. Ann Nucl Med. 2013;27:11–6.
19. Herzog BA, Buechel RR, Katz R, Brueckner M, Husmann L, Burger IA, et al. Nuclear myocardial perfusion imaging with a cadmium–zinc–telluride detector technique: optimized protocol for scan time reduction. J Nucl Med. 2010;51:46–51.
20. Hindorf C, Oddstig J, Hedeer F, Hansson MJ, Jogi J, Engblom H. Importance of correct patient positioning in myocardial perfusion SPECT when using a CZT camera. J Nucl Cardiol. 2014;21:695–702.
21. Fiechter M, Gebhard C, Fuchs TA, Ghadri JR, Stehli J, Kazakauskaite E, et al. Cadmium–zinc–telluride myocardial perfusion imaging in obese patients. J Nucl Med. 2012;53:1401–6.
22. Gimelli A, Bottai M, Giorgetti A, Genovesi D, Filidei E, Marzullo P. Evaluation of ischaemia in obese patients: feasibility and accuracy of a low-dose protocol with a cadmium–zinc telluride camera. Eur J Nucl Med Mol Imaging. 2012;39:1254–61.
23. Herzog BA, Buechel RR, Husmann L, Pazhenkottil AP, Burger IA, Wolfrum M, et al. Validation of CT attenuation correction for high-speed myocardial perfusion imaging using a novel cadmium–zinc–telluride detector technique. J Nucl Med. 2010;51:1539–44.
24. Mouden M, Timmer JR, Ottervanger JP, Reiffers S, Oostdijk AH, Knollema S, et al. Impact of a new ultrafast CZT SPECT camera for myocardial perfusion imaging: fewer equivocal results and lower radiation dose. Eur J Nucl Med Mol Imaging. 2012;39:1048–55.
25. Fiechter M, Ghadri JR, Kuest SM, Pazhenkottil AP, Wolfrum M, Nkoulou RN, et al. Nuclear myocardial perfusion imaging with a novel cadmium–zinc–telluride detector SPECT/CT device: first validation versus invasive coronary angiography. Eur J Nucl Med Mol Imaging. 2011;38:2025–30.
26. Buechel RR, Pazhenkottil AP, Herzog BA, Husmann L, Nkoulou RN, Burger IA, et al. Real-time breath-hold triggering of myocardial perfusion imaging with a novel cadmium–zinc–telluride detector gamma camera. Eur J Nucl Med Mol Imaging. 2010;37:1903–8.
27. Gimelli A, Bottai M, Quaranta A, Giorgetti A, Genovesi D, Marzullo P. Gender differences in the evaluation of coronary artery disease with a cadmium–zinc telluride camera. Eur J Nucl Med Mol Imaging. 2013;40:1542–8.